A Volterra Type Model for Image Processing

Georges Henri Cottet and Mohamed El Ayyadi

***Abstract*—We present a class of time-delay anisotropic diffusion models for image restoration. These models lead to asymptotic states that are selected on the basis of a contrast parameter and bear some analogy with neural networks with Hebbian dynamical learning rules. Numerical examples show that these models are efficient in removing even high levels of noise, while allowing an accurate tracking of the edges.**

***Index Terms*— Adaptive neural network, image restoration, nonlinear diffusion, selective filter, time-delay regularization.**

I. Introduction

In RECENT years diffusion models for image restoration have received much attention from mathematicians. Since the pioneering work of Perona and Malik [12], a great deal of work has been done in particular toward the derivation of efficient adaptive, nonlinear, diffusion partial differential equations (PDE's).

The goal of these models is to selectively filter the images without losing significant features. In some cases, contrast enhancement is also sought as a desirable property of the filter. One common trend in all these models is the need to embed them within a mathematically sound theoretical framework. The motivation for that is twofold. First, it is natural to require the model to reproduce some natural features of image processing which can be easily translated into mathematical terms, e.g., maximum principle, monotony. Second, a mathematical framework is necessary to make sure that discretizations of the model itself will retain most of its properties.

One striking illustration of this mathematical approach is the fundamental work of [1], where a class of PDE's of mean curvature type is rigorously analyzed in the light of natural axioms for multiscale image processing. For other recent works on nonlinear diffusion for image filtering, we refer to [2], [3], [13], [14].

In the models generally discussed in the literature, the time variable is connected to space scales and the diffusion equation yields a continuous range of filters acting within the corresponding scales. Our paper deals with a different approach for the construction of efficient filters. Rather than providing a multiscale description of the image, we will consider the image as a perturbation of a unique "true" image that we wish to restore, in a way that does not require from the user the definition of any stopping time, something which in practice can be difficult to *a priori* decide.

Manuscript received August 7, 1996; revised March 6, 1997. The associate editor coordinating the review of this manuscript and approving it for publication was Dr. Guillermo Sapiro.

The authors are with LMC-IMAG, Université de Grenoble, 38041 Grenoble Cédex 9, France (e-mail: cottet@imag.fr).

Publisher Item Identifier S 1057-7149(98)01750-3.

We are thus looking for a dynamical system equipped with a satisfactory attractor. By satisfactory, we mean that it should be large enough to contain the images we wish to restore, while allowing the basin of attraction of these to extend to images deteriorated by a significant level of noise. We also wish to avoid as much as possible the notion of minimal scale or to keep it as small as possible, typically the minimal number of pixels necessary to detect coherent patterns within the image.

Our model results from the combination of two tools: anisotropic nonlinear diffusion and time-delay regularization. Although not as popular as the above mentioned techniques, these tools have indeed already been considered in the literature. Anisotropic diffusion tensors lead to models where the anisotropy is built-in rather than resulting from the geometry of the image itself. They have been used in combination with reaction terms [7] or in the context of multiscale image analysis [15]. Compared to scalar diffusion models they seem to allow a more accurate tracking of the edges.

On the other hand, time-delay regularization is an alternative to spatial regularization in the construction of diffusion coefficients from the image itself, which has already been proposed to stabilize the Perona–Malik model [11].

The originality of our approach lies in the combination of these two tools and in the form of the forcing term in the time-delay equation governing the diffusion matrix. Our guideline to choose an efficient time-regularization has been the analogy between PDE's of diffusion type and neural networks [4], [9]. This analogy results from integral approximations of diffusion equations and allows to translate the diffusion tensor in terms of synaptic weights linking neurons lying within a short synaptic range. While neural networks are particularly appealing in the context of signal processing, we believe that their PDE counterparts yield a more immediate intuition on how the relevant parameters affect their dynamics. Motivated by this observation we were looking for PDE's with time-delay regularization that would translate, at the continuous level, natural learning rules in neural networks. These so-called Hebbian learning rules allow to dynamically either enhance or decrease the connections between nearby neurons, depending on the coherence of the activities of these neurons as observed on a certain time window.

As a matter of fact, while our first choice was actually directly inherited from the spatial regularization used in [7], it was recognized that this model was related to a neural network where, in the learning rule, the coherence of the neurons was not evaluated in a satisfactory way [5]. Moreover a threshold parameter, necessary to distinguish between coherence and noise, was missing in this model. In the final model we present here, such a contrast parameter is introduced, with the effect of

selecting steady states: These steady states consist in images made of homogeneous patterns (with constant grey levels), separated by fronts with stiffness controlled by the contrast parameter. In the applications we have considered, this class of steady states proved to fulfill our goals. The analogy with neural networks proved also useful in suggesting a strategy by which the diffusion tensor obtained on a first steady-state is reinjected together with the original unprocessed image for a new calculation cycle. We believe that this possibility is a striking feature that distinguishes time-delay from spatial regularization. In practice, our calculations indicate that it allows image restoration on fine scales even when starting from highly degraded images.

The outline of this paper is as follows. In Section II, we present our model in a general abstract form and prove some mathematical results, namely its well-posedness when additional spatial smoothing is used in the construction of the diffusion tensor. Section III focuses on the particular model we just sketched. We discuss the various parameters involved in the model, describe our numerical discretization and give numerical illustrations based both on synthetic and natural images. In Section IV, we briefly derive the neural network approximation of a related diffusion model. This model differs from the one presented in the previous section essentially by allowing antidiffusion and, thus, strong contrast enhancement. Although its well-posedness is questionable, it turns out that its discrete neural network implementation exhibits a Lyapunov function and thus can be proved to lead to stable steady-state asymptotics.

In closing this introduction, let us mention that, although we focus here on two-dimensional (2-D) applications, all the ideas presented here readily extend to three dimensions. Applications for three-dimensional (3-D) image processing will be presented elsewhere.

II. The Abstract PDE Model

Let us consider an initial image in the unit square $\Omega =]-1, +1[^2$ whose grey level is given by a function u_0 with values in $[-1, +1]$. Our filter is based on the following general system of partial differential equations:

$$\frac{\partial u}{\partial t} - \operatorname{div}(L\nabla u) = 0 \tag{1}$$

$$\frac{\partial L}{\partial t} + L = F(\nabla_\sigma u) \tag{2}$$

where

$$\nabla_\sigma u = \nabla(u \star f_\sigma), \quad f_\sigma(y) = \sigma^{-2} f\Big(\frac{y}{\sigma}\Big), \quad \int f\,dx = 1.$$

This system has to be supplemented with initial values u_0 and L_0 and periodic boundary conditions. As a matter of fact, boundary conditions are not an important issue in image processing and periodic boundary conditions are only dictated by our wish to get rid of any technical unessential difficulties. In particular, it will enable us to avoid boundary terms in the integrations by parts encountered in the sequel.

In the above system L and F are 2×2 matrices. Although the precise form of F will be discussed later, one can already recognize that (1) is an anisotropic diffusion equation and that the diffusion matrix takes into account information, as time goes on, from the gradient of u.

As for σ, it is a positive smoothing parameter needed for the mathematical well-posedness of the system, although in practice the value $\sigma = 0$ (for which $\nabla_\sigma = \nabla$) proved to be satisfactory. In any case it is important to emphasize immediately that this parameter should be considered as case independent, in contrast with other diffusion models (for instance, [3] and [7]), where the smoothing parameter has to be adjusted in particular to the noise level of the image. The model parameters which are relevant for practical applications are discussed in Section III.

Let us now indicate the smoothness assumptions on f and F that we will make throughout this paper:

F is a nonnegative symmetric matrix:

$$\langle F(v)w, w\rangle \geq 0, \qquad \forall v, w \in \mathbb{R}^2 \tag{3}$$

F and its derivatives are bounded:

$$|F(v)| + |\nabla F(v)| \leq C, \qquad \forall v \in \mathbb{R}^2 \tag{4}$$

f and its derivatives are bounded. (5)

The goal of (3) is clearly to avoid antidiffusion in (1): if one starts from a positive diffusion matrix

$$L_0 \geq \alpha \mathrm{Id}, \qquad \alpha > 0 \tag{6}$$

the explicit integration of (2), combined with (3) yields

$$L(\cdot, t) \geq \alpha e^{-t}\mathrm{Id}$$

and (1) is a parabolic equation. The rest of this section is devoted to the proof of the following result:

Theorem 1: Assume $(u_0, L_0) \in L^\infty(\Omega) \times [L^\infty(\Omega) \cap H^1(\Omega)]^4$ and L_0 satisfies (6). Then the system (1) and (2) has, for $\sigma > 0$, a unique solution satisfying, for $T > 0$

$$u \in L^2[0, T; H^1(\Omega)] \cap L^\infty[0, T; L^\infty(\Omega)];$$
$$L \in L^\infty\{0, T; [L^\infty(\Omega) \cap H^1(\Omega)]^4\}. \tag{7}$$

Our strategy to prove the existence of a solution will be based on compactness arguments: We will construct approximate solutions and derive *a priori* estimates, which will enable us to pass to the limit and get a solution to our problem. A simple way to construct approximate solutions is to work on retarded–mollified versions of (1) and (2).

More precisely, we proceed as follows. We first extend the initial conditions L_0 and u_0 to negative times. Then, given a small parameter h and a one-dimensional smooth cut-off function χ with support in $]-2, -1[$ and integral 1, we set

$$\chi_h(t) = \frac{1}{h}\chi\Big(\frac{t}{h}\Big)$$

and we denote by $\star_t$ the convolution with respect to the time variable. We now look for u_h and L_h solutions to

$$\frac{\partial u_h}{\partial t} - \operatorname{div}([L_h \star_t \chi_h]\nabla u_h) = 0 \tag{8}$$

$$\frac{\partial L_h}{\partial t} + L_h = F(\nabla_\sigma u_h). \tag{9}$$

Dividing the time interval into time steps of size h and using a straightforward induction argument confirms that this problem is well-posed [the time delay introduced by the cut-off is actually nothing else than an explicit, with respect to the nonlinear terms, time-discretization of the original equation (1)].

To be able to pass to the limit as h tends to zero, we need *a priori* estimates on (u_h, L_h). Such estimates can easily be derived due to the parabolic nature of (8).

Lemma 2: Let $T > 0$. Then

$$L_h \text{ is bounded in } L^\infty\{0, T; [L^\infty(\Omega) \cap H^1(\Omega)]^4\}; \tag{10}$$

$$L_h \text{ is uniformly positive-definite for } t \le T; \tag{11}$$

$$u_h \text{ is bounded in } L^\infty[0, T; L^\infty(\Omega)] \cap L^2[0, T; H^1(\Omega)]. \tag{12}$$

Proof: Integrating (9) yields

$$L_h(t) = e^{-t} L_0 + \int_0^t e^{s-t} F[\nabla_\sigma u_h(\cdot, s)]\, ds$$

which, by (3), (4), and (6), implies

$$|L_h(x, t)| \le C;\ L_h(x, t) \ge \alpha e^{-T} \mathrm{Id} \quad \forall x \in \Omega, -\infty < t < T$$

[recall that $L_h(t) = L_0$ for negative t]. Since χ is nonnegative and is bounded, this implies

$$|L_h \star_t \chi_h| \le C;\ L_h \star_t \chi_h \ge \alpha e^{-T} \mathrm{Id} \quad \forall x \in \Omega, -\infty < t < T.$$

This proves the L^∞ bound in (10), and (11), and enables us to apply the maximum principle to obtain the L^∞ bound in (12). To get the H^1 estimate in (12), we classically multiply (8) by u_h and integrate over Ω to obtain

$$\frac{1}{2} \frac{d}{dt} ||u_h||_{L^2}^2 + \langle [L_h \star_t \chi_h] \nabla u_h, \nabla u_h \rangle = 0$$

and, after integrating in time

$$\alpha e^{-T} \int_0^T ||\nabla u_h(\cdot, s)||_{L^2}^2\, ds \le \int_0^T \int_\Omega \langle [L_h \star_t \chi_h] \nabla u_h, \nabla u_h \rangle\, dt \le 1/2 ||u_0||_{L^2}^2.$$

Finally, to obtain the H^1 estimate in (10), we differentiate (9) to get (with the notation ∂_i for $\partial/\partial x_i$)

$$\frac{\partial}{\partial t} (\partial_i L_h) + \partial_i L_h = \sum_j (\partial_i u_h \star \partial_j f_\sigma) \frac{\partial F}{\partial u_j} (\nabla_\sigma u_h).$$

Using (4), (5) and multiplying the above equation by $\partial_i L_h$ we obtain

$$\frac{d}{dt} ||\partial_i L_h||_{L^2}^2 \le C ||\nabla u_h||_{L^2}^2$$

from which the H^1 estimate for L_h follows. ∎

Thanks to the *a priori* estimates just proved, we are now able to give the following result, where Q stands for $]0, T[\times\Omega$.

Lemma 3: There exists a subsequence, still noted (L_h, u_h), and (L, u) satisfying (7) such that

$$L_h \to L \text{ strongly in } L^2(Q); \tag{13}$$

$$u_h \to u \text{ strongly in } L^2(Q) \text{ and weakly in } L^2[0, T; H^1(\Omega)]; \tag{14}$$

$$F(\nabla_\sigma u_h) \to F(\nabla_\sigma u) \text{ strongly in } L^2(Q). \tag{15}$$

Proof: The two first assertions easily follow, through classical compactness properties, from (10) and (12), if in addition we observe that, due to (8)–(10) and (12), $\partial u_h/\partial t$ and $\partial L_h/\partial t$ are, respectively, bounded in $L^2[0, T; H^{-1}(\Omega)]$ and $L^2(Q)$. Assertion (15) then easily follows from (14) and the smoothness of F. ∎

It is now straightforward to pass to the limit in (8) and (9), and in particular in the right hand side of (9), and in the nonlinear term of (8), to obtain that (u, L) is a weak solution to our system.

Let us now prove the uniqueness of the solution. Let (u, L) and (v, M) be two solutions and set $e = u - v$, $E = L - M$. By subtraction, we have $E(\cdot, 0) = e(\cdot, 0) = 0$ and

$$\frac{\partial e}{\partial t} - \mathrm{div}(M \nabla e) = -\mathrm{div}(E \nabla u) \tag{16}$$

$$\frac{\partial E}{\partial t} + E = F(\nabla_\sigma u) - F(\nabla_\sigma v). \tag{17}$$

Multiplying (16) by e we obtain, for $t \le T$

$$\begin{aligned} \frac{1}{2} \frac{d}{dt} ||e||_{L^2}^2 + \alpha e^{-T} ||\nabla e||_{L^2}^2 &\le ||E \nabla u||_{L^2} ||\nabla e||_{L^2} \\ &\le \frac{1}{2} \left(\frac{e^T}{\alpha} ||E \nabla u||_{L^2}^2 + \alpha e^{-T} ||\nabla e||_{L^2}^2 \right) \end{aligned}$$

and therefore

$$\frac{d}{dt} ||e||_{L^2}^2 \le C ||E \nabla u||_{L^2}^2 \le C ||E||_{L^\infty}^2 ||\nabla u||_{L^2}^2. \tag{18}$$

From (4) and (17) we deduce that

$$\begin{aligned} ||E(\cdot, t)||_{L^\infty} &\le C \int_0^t ||e(\cdot, s) \star \nabla f_\sigma||_{L^\infty}\, ds \\ &\le C \int_0^t ||e(\cdot, s)||_{L^2}\, ds \end{aligned}$$

and (18) yields

$$||e(\cdot, t)||_{L^2}^2 \le C \int_0^t ||\nabla u(\cdot, s)||_{L^2}^2\, ds \int_0^t ||e(\cdot, s)||_{L^2}^2\, ds.$$

Since $\nabla u \in L^2(Q)$, this implies that $e \equiv 0$, and thus $E \equiv 0$.

Note that, as a by-product, the uniqueness proof gives also the continuous dependence of the solution on the initial conditions. Together with the conservation of the mean grey value, which results from the conservative form of (1), and the maximum principle, this is a desirable qualitative feature for any diffusion model. Let us point out that, as we will see below, the model has no monotony property. In closing this section, we now shortly comment on the important case $\sigma = 0$,

that is when (2) does not induce any spatial smoothing. After explicit integration of (2), our system can be rewritten as

$$\frac{\partial u}{\partial t} - e^{-t}\,\mathrm{div}(L_0\nabla u) - \int_0^t e^{s-t} \cdot \mathrm{div}\{F[\nabla u(\cdot, s)]\nabla u(\cdot, t)\}\,ds = 0.$$

This is a Volterra equation. This kind of equation is typically involved in modeling fluids or material with memory. However, our model has some specific features that do not seem to have been addressed in the literature, namely the fact that the time variables t and s are coupled in the divergence term inside the time integral, and the strong nonlinearity introduced by F. These features seem to preclude the use of classical monotony or fixed point arguments. So far, we were unable to extend to this case the compactness arguments employed in our proof for $\sigma > 0$.

III. Applications

In the discussion below as well as in all the calculations to follow, the parameter σ has been taken equal to zero. We do not think that taking a positive value would have an important impact on our numerical results, as long as σ would remain small. As a matter of fact, taking for f a tensor product of hat functions and for σ the pixel resolution of the image, would lead to an evaluation of $\nabla_\sigma u$ through the trapezoidal rule which coincide with the usual centered finite difference formula for ∇u. However, it is fair to mention that the steady states discussed below for $\sigma = 0$, and observed in our computations, would not strictly speaking persist for $\sigma > 0$.

In this section, we first specify the right hand side of (2) and discuss the choice of the various parameters in our model, then show some numerical experiments.

A. Choice of F and Relaxation Time in (2)

As already mentioned, our choices are dictated by our wish to prevent diffusion across the significant edges of the image. The distinction between significant edges and high gradient zones resulting from noise will be classically based on averaging. Our first choice is

$$F_0(\nabla u) = \mathbb{P}_{\nabla u^\perp} \tag{19}$$

(orthogonal projection on the direction orthogonal to the gradient of the image).

In two dimensions, this means that, with the notation $\nabla u = (u_1, u_2)$

$$F = |\nabla u|^{-2}\begin{bmatrix} u_2^2 & -u_1u_2 \\ -u_1u_2 & u_1^2 \end{bmatrix}.$$

We also introduce a time scale factor τ in the relaxation equation (2) so that the evolution equation for the diffusion tensor reads

$$\frac{\partial L}{\partial t} + \frac{1}{\tau}L = \frac{1}{\tau}F_0(\nabla u). \tag{20}$$

Roughly speaking, the meaning of (20) is that the diffusion direction is a time average, over a time scale of τ, of the directions perpendicular to the edges, while the effect of the initial choice for L fades away. This model is reminiscent to the one introduced in [7], where these directions where based on space (rather than time) averages of the gradients. One advantage we found in this new model however is that it allows for stable steady states, while in the model of [7] the diffusion equation had to be supplemented with a reaction term to allow to obtain the processed image on the asymptotic states. In practice the choice of the levels of the reaction term is not always straightforward, and we could experience that a pure diffusion equation is more tractable than a reaction-diffusion equation.

Our next choice results from the observation that (19) actually leads to too many steady states (clearly, any image together with the diffusion tensor along directions perpendicular to the edges is a steady state), reducing henceforth the attraction basins of these steady states. In practice we have observed that, when used on an image perturbed with a high noise level, this filter converges too fast and the processed image retains a substantial amount of noise [note in addition that F_0 does not satisfy (4)].

To overcome this difficulty we have chosen to select the steady states on the basis of a contrast threshold parameter. We define

$$F_s(\nabla u) = \begin{cases} \mathbb{P}_{\nabla u^\perp} & \text{if } |\nabla u| \geq s \\ \dfrac{3}{2}\left(1 - \dfrac{|\nabla u|^2}{s^2}\right)\mathrm{Id} + \dfrac{|\nabla u|^2}{s^2}\,\mathbb{P}_{\nabla u^\perp} & \text{if not} \end{cases}. \tag{21}$$

When the gradients are not large enough (as seen on a time span of τ) the diffusion matrix will thus still be fed with isotropic diffusion, allowing to further filter the image away from the edges. We refer to Section IV for the explanation of the specific form chosen for the right hand side above, and in particular the coefficient 3/2.

By considering images such that $L\nabla u = 0$ where L has the form of the right hand side above, one easily finds that the steady states resulting from this model are images made of homogeneous patterns separated by fronts of stiffness larger than s (of course, as we already said, these steady states would not persist for $\sigma > 0$).

While the parameter s has a clear meaning in our system, there are two additional parameters that need to be clarified: the initial diffusion matrix L_0 and the relaxation time τ. Concerning the first one, it is easy to verify that the only relevant parameter is the coercivity parameter α which governs the amount of initial dissipation in the system (refer to the mathematical analysis in Section II). Moreover, through appropriate time change of variables, one can switch from one initial diffusion matrix to another by changing the relaxation time. Notice that one is only interested in asymptotics of the system, and, unlike for multiscale diffusion models, we are not interested in transient states. We can thus assume that L_0 is, say, the identity and restrict our discussion to the relaxation parameter τ.

This relaxation parameter can actually be related to a minimal scale parameter, as shown by the following simple calculation. Assume several homogeneous patterns organized in concentric rings inside a ball ω of radius ε, so that ∇u vanishes for all time on the boundary of ω. To check for the possibility for the fronts to be preserved inside ω we look at the difference between u and its mean value $\overline{u}$ in ω. First we observe that, in view of the conservative form of (1) and of the fact that $\nabla u = 0$ on the boundary of ω, $\overline{u}$ remains constant. If we set $e = u - \overline{u}$, we thus have

$$\frac{\partial e}{\partial t} - \operatorname{div}(L\nabla e) = 0.$$

We have assumed that $L_o = \mathrm{Id}$, therefore $L \geq e^{-t/\tau}\mathrm{Id}$. Multiplying by e and integrating by part we thus get

$$\frac{d}{dt}\,\|e\|_{L^2}^2 + e^{-t/\tau}\|\nabla e\|_{L^2}^2 \leq 0.$$

Now by the Poincaré inequality we have

$$\|\nabla e\|_{L^2}^2 \geq c\varepsilon^{-2}\|e\|_{L^2}^2$$

where c is a constant independent of ε, and Gronwall's theorem yields

$$\|e\|_{L^2}^2 \leq \|e_0\|_{L^2}^2 \,\exp\left\{c\,\frac{\tau}{\varepsilon^2}[e^{-t/\tau} - 1]\right\}.$$

As a result we get

$$\|e\|_{L^2} \to \|e_0\|_{L^2} \,\exp\frac{-c\tau}{\varepsilon^2}.$$

This means that patterns on scales which are small compared to $\sqrt{\tau}$ are averaged out, or, in other words, that fronts will spread on scales of the order of $\sqrt{\tau}$.

From this point of view, our parameter τ can be related to stopping times involved in multiscale filters, with, however, the crucial difference that, where the filter does not detect coherent fronts, the right hand side of (21) still contains isotropic diffusion, allowing to keep removing noise within each detected coherent pattern. In practice, as we will see in the numerical examples which follow, we found this feature very important to allow for efficient noise reduction together with preservation of fine scale coherent patterns.

To summarize, our filter acts as follows: In a first smoothing stage, gradient directions are detected; then, within each pattern surrounded by a stiff enough front, grey values are averaged, enhancing the contrast with the neighboring patterns (the nonmonotony of our model is apparent here: large grey values with no-contrast will be washed out, while smaller grey values, but with sufficient contrast, will be preserved).

B. Numerical Examples

Let us first briefly describe our numerical procedure. Equation (1) is discretized by using classical one-sided difference schemes for the operators divergence and ∇, together with an explicit time-discretization. If we denote by u_{pq} the value of u at the pixel $(x = ph, y = qh)$ we set

$$\Delta_+^x u_{p,q} = u_{p+1,q} - u_{p,q}, \quad \Delta_-^x u_{p,q} = u_{p,q} - u_{p-1,q}$$

and similar formulas for finite-differences in the y direction. Let us denote by

$$[L_{pq}]_{xx}, \quad [L_{pq}]_{yx}, \quad [L_{pq}]_{xy}, \quad [L_{pq}]_{yy}$$

the entries of the diffusion tensor L at the pixel (ph, qh) and use superscripts to refer to time levels. The time step is denoted by Δt. Then (1) is solved by

$$\frac{u_{pq}^{n+1} - u_{pq}^n}{\Delta t} - \frac{\Delta_+^x([L_{pq}]_{xx}^n \Delta_-^x u_{pq}^n + [L_{pq}]_{xy}^n \Delta_-^y u_{pq}^n)}{h^2} - \frac{\Delta_+^y([L_{pq}]_{yx}^n \Delta_-^x u_{pq}^n + [L_{pq}]_{yy}^n \Delta_-^y u_{pq}^n)}{h^2} = 0. \tag{22}$$

Note that, for a scalar tensor L, these formulas yield the classical 5-points box. As for (20), it is solved by the semi-implicit scheme:

$$\frac{L^{n+1} - L^n}{\Delta t} + \frac{L^{n+1}}{\tau} = \frac{F^n}{\tau}$$

which gives

$$L_{pq}^{n+1} = \left(\frac{1}{1+\beta}\right)(\beta L_{pq}^n + F_{pq}^n) \tag{23}$$

where $\beta = \tau/\Delta t$ and F_{pq} is computed on the basis of (21) with gradients obtained through centered finite differences.

The reason for choosing this time-discretization is that, since F is positive, it enforces that L is at all time step positive definite. Therefore, if we rewrite (22) in the matrix form

$$u^{n+1} = \left[\mathrm{Id} + \frac{\Delta t}{h^2} M\right] u^n$$

it easily results from discrete integration by parts (which as a matter of fact are made possible by the combined use of Δ_+ and Δ_- finite difference formulas) that M is a positive definite matrix. We thus have a L^2-stable scheme, as soon as

$$\Delta t \leq \frac{2}{\lambda_{\max}}\, h^2$$

where $\lambda_{\max}$ is the maximum eigenvalue of M. Looking at the entries of M as given from (22), a crude estimate of this quantity is $16 \max_{p,q}\{|[L_{pq}]_{xx}|, |[L_{pq}]_{yx}|, |[L_{pq}]_{xy}|, |[L_{pq}]_{yy}|\}$. Our time step is updated at every time on the basis of this estimate (as time goes on, this actually yields only minor variations of the time step).

We now come to our first example, which is the classical *triangle over rectangle* image. This example will enable us to illustrate the point of view on image processing emphasized in the introduction, namely that our goal is to recover underlying exact images on the asymptotics of our PDE system.

Given a black and white image where a proportion r of the pixels have been replaced by random values, we will compare in energy norm, the results of our algorithm with the exact image where the grey levels are $1 - r$ and $-1 + r$. Fig. 1 shows the result for a 128×128 image and $r = 0.7$ (that is a noise level of 70%). The parameters used in this calculation are $\tau = 10\Delta t$, and $s = 5$. This value of s corresponds to a maximal spreading of the fronts connecting grey levels 0.3 to -0.3 over about 13 pixels. The bottom pictures show the residual (difference between the images at two successive

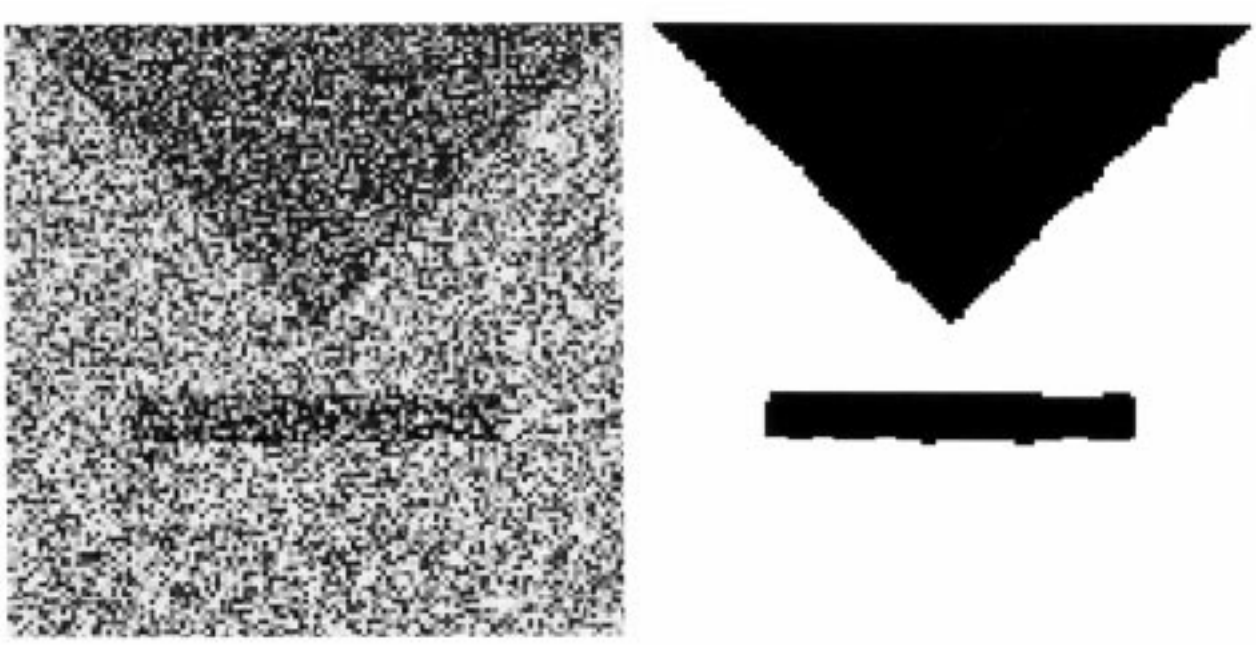

Fig. 1. 128 × 128 triangle–rectangle image with 70% noise (left), and the processed image after thresholding (right). Parameters are $\tau = 10\Delta t$, $s = 5$.

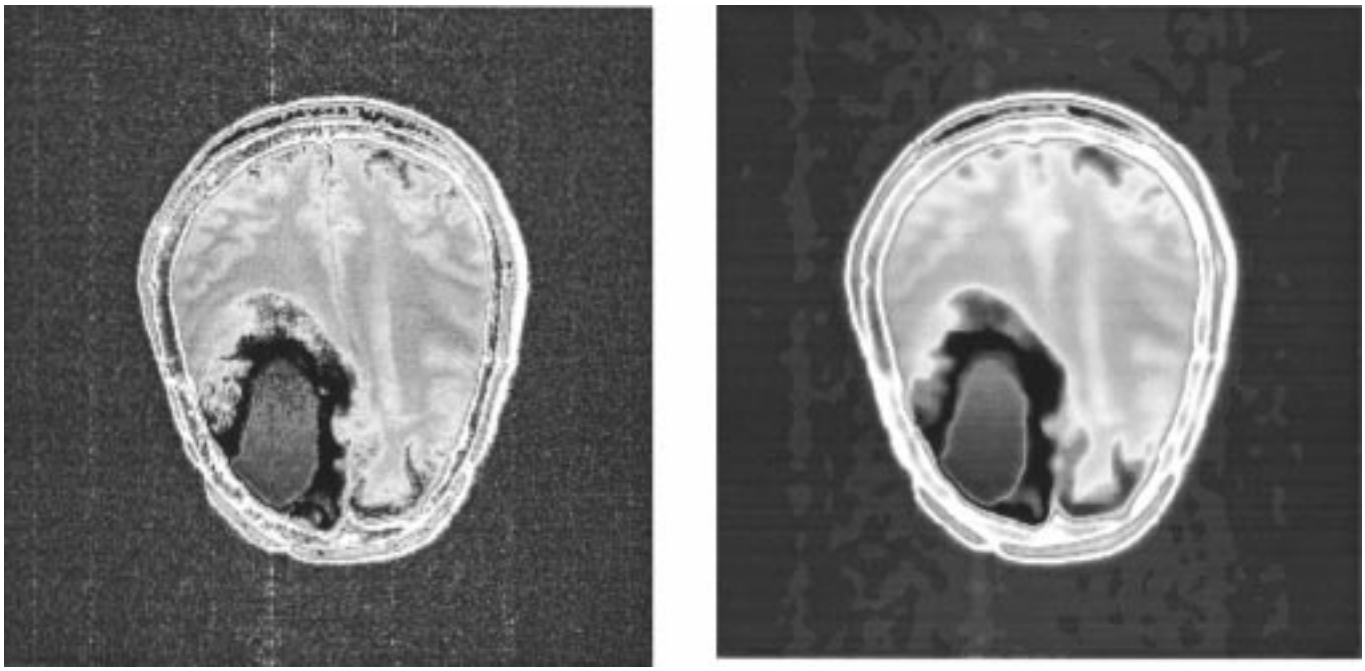

Fig. 2. 256 × 256 MRI image. Left: original. Right: processed image. Parameters are $\tau = 3\Delta t$, $s = 5$.

iterations) in a logarithmic scale and the error. These curves illustrate the convergence of the result of our model to a steady state. The top right picture shows a thresholded version of the result of the algorithm after 100 iterations. One can see that, except for two locations, the edges are accurately recovered within one pixel. Let us stress the fact that the rectangle below the triangle is rather narrow (ten pixels wide).

Our second example is a 256 × 256 medical resonance image (MRI) of the brain (left picture of Fig. 2). The processed image (right picture) shows the relevant coherent zones in the image, corresponding to homogeneous tissues in the tumor, and the compressed zones of the brain around it. This result compares well to that obtained by the reaction–diffusion method in [7], with the difference that here it was not necessary to *a priori* select the grey levels of the asymptotics to tune the reaction term. The parameter used in this calculation were $\tau = 3\Delta t$ and $s = 5$. Due to the relatively small amount of noise in this image, our calculation converged (on the basis of a residual threshold of 10^{-4}) in ten iterations.

We borrowed our two next examples from Weickert's thesis [16]. In the first one (left column of Fig. 3) the goal is to extract the light, coherent quasi-one dimensional (1-D) curve

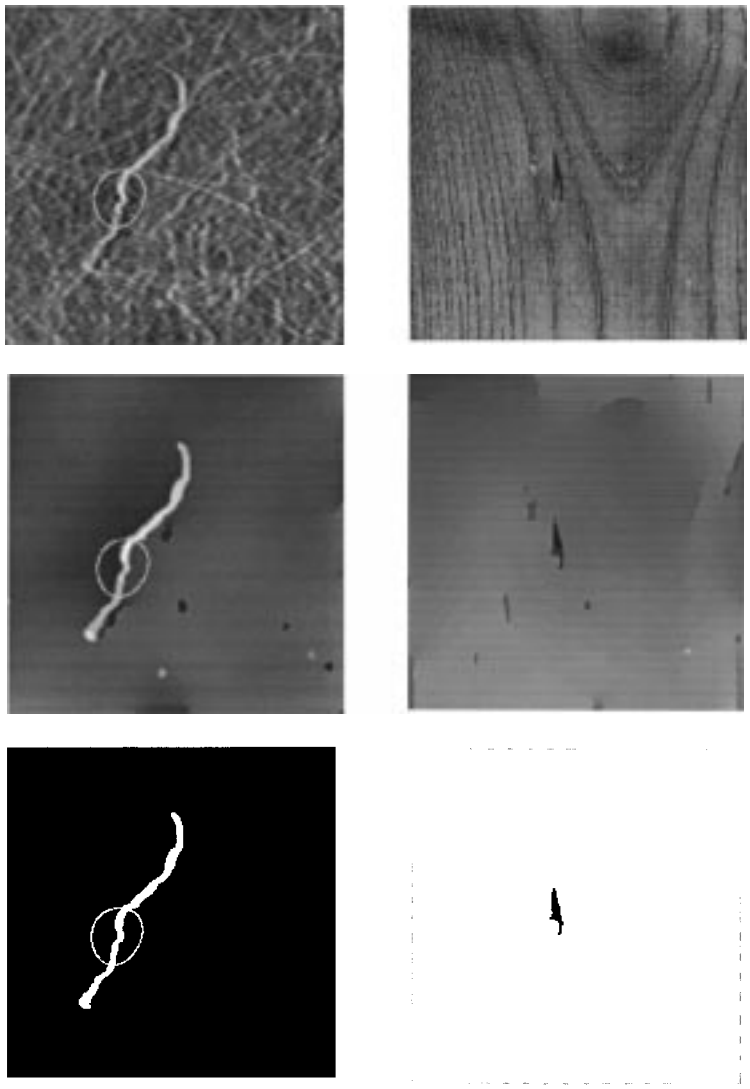

Fig. 3. Image processing on a fabric image (left column) and a wood surface image (right column). Top: original image. Middle: processed images, (respectively, with $\tau = 6\Delta t$, $s = 9$ and $\tau = 4\Delta t$, $s = 6$). Bottom: processed images after thresholding.

in the middle of the picture. This could be done on the basis of our contrast parameter whose value was chosen as six. The relaxation time was $4\Delta t$. The top picture shows the original image, the middle one gives the processed image after 300 iterations, and the bottom one is what results from a thresholding of this image. It must be pointed out that selecting a smaller value of τ would extract more fine scale structures, but not affect edges obtained here. One conclusion that can be drawn from this calculation, is that our filter is able to achieve a substantial amount of smoothing in non coherent zones, while respecting very well fine coherent structures (see the circled area in the pictures, where the curvature of the white curve is rather well preserved).

The same observation can be made from the right pictures of Fig. 3, which show how some defect in a piece of wood can be successfully extracted by our algorithm (note the small right leg of the defect).

We now come to more challenging tests, which combine high noise levels with fine scale details. First we go back to the triangle–rectangle example with a noise level of 90%. In this case we had to widen slightly the rectangle (twelve pixels instead of ten). Below this value, it seems that the statistics of the random generator could not allow to recognize any kind of coherence. Due to the high level of noise, we had either to take a large value of τ or a large value of s to allow sufficient amount of Gaussian filter in the diffusion tensor. In the experiment we show, we took $\tau = 10$, as for the 70% case, and $s = 13$ (notice, however, that similar results were obtained by taking $s = 5$, like in the 70% case, and $\tau = 20$). A direct implementation of our code resulted in a spreading of the fronts in the initial stage of the computation, which eventually destroyed the already small contrast of the image. The edges of the rectangle could not resist to this processing. An interpretation of this is that, in these parameter ranges, the behavior of the algorithm is very sensitive to the initial dissipation choice in L_0.

To overcome this difficulty, we used the following procedure, using the same parameters as above: once the residual falls below some threshold, yielding a first asymptotic state $(\overline{u}, \overline{L})$, we restart the algorithm with initial values u_0 and

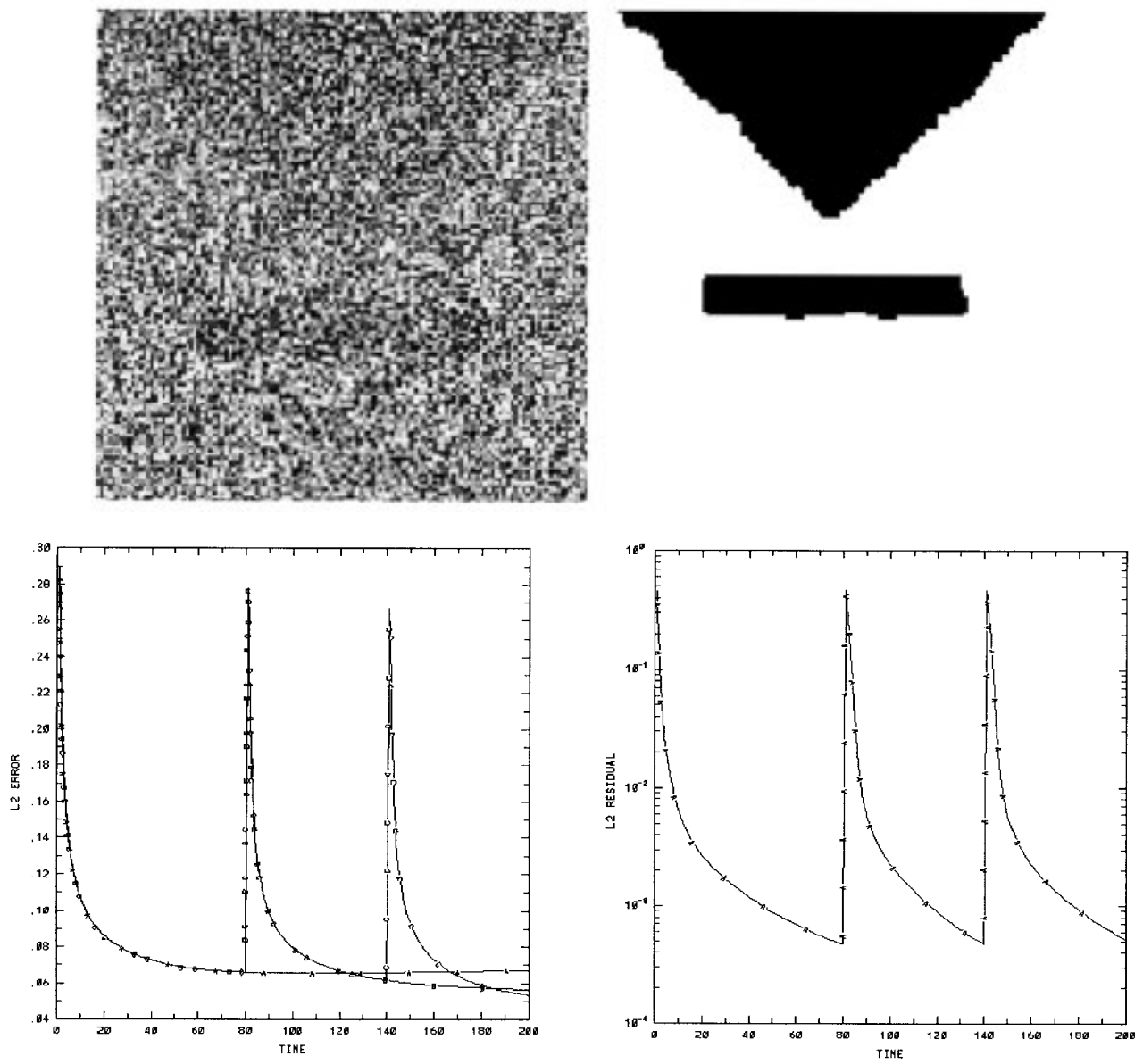

Fig. 4. 128 × 128 triangle–rectangle image with 90% noise. Top-left: original image. Top-right: processed image after thresholding. Bottom-left: L2 error. Bottom-right: residual; curves A, B, C correspond to zero, one, or two reinitializations. Parameters are $\tau = 10\Delta t$, $s = 5$.

$\overline{L}$. It is not difficult to check that, provided the fronts do not spread beyond the contrast threshold parameter, this procedure does recover exactly the steady states of the model.

We believe that this idea is indeed rather natural, in particular in view of the analogy (see Section IV) between our filter and neural networks: It means that, while processing the signal and adapting its connections, the network is able to recall at any time the original information it had to deal with. Moreover, it is worth noticing that this procedure can be repeated automatically on the basis of a residual threshold, which makes it simple to use. In some sense, the effect of this iterative process is to make the ultimate asymptotic states essentially independent of the initial choice of L_0. The bottom-left picture in Fig. 4 shows the effect of two reinitializations on the decay of the error. In the thresholded image (top-right picture) one can recognize that, even if the result is clearly not as good as for the 70% case, the edges have been reasonably well restored.

Our next example is a landscape image (see Fig. 5) that has been degraded by noise at a 30% level, then processed in two successive sweeps. While the first steady state shows a reasonable result on large scale patterns, the second sweeps has dramatically improved the restoration of fine scale details (like the windows in the wall of the main building in the foreground).

Our final example will be an ultrasound image. This kind of image combines high-level noise and low contrast, which makes it difficult to deal with. The top-left picture of Fig. 6 is the original image, the top-right is the first asymptotic, and the bottom picture is the result of restarting the algorithm afterwards. One can see in the last picture a better preservation of the edges in the bottom part of the darkest area, and, what is more important in this particular image, of the intermediate grey large structure (prostate) underneath. The combination of our filter with snake-splines techniques has actually allowed

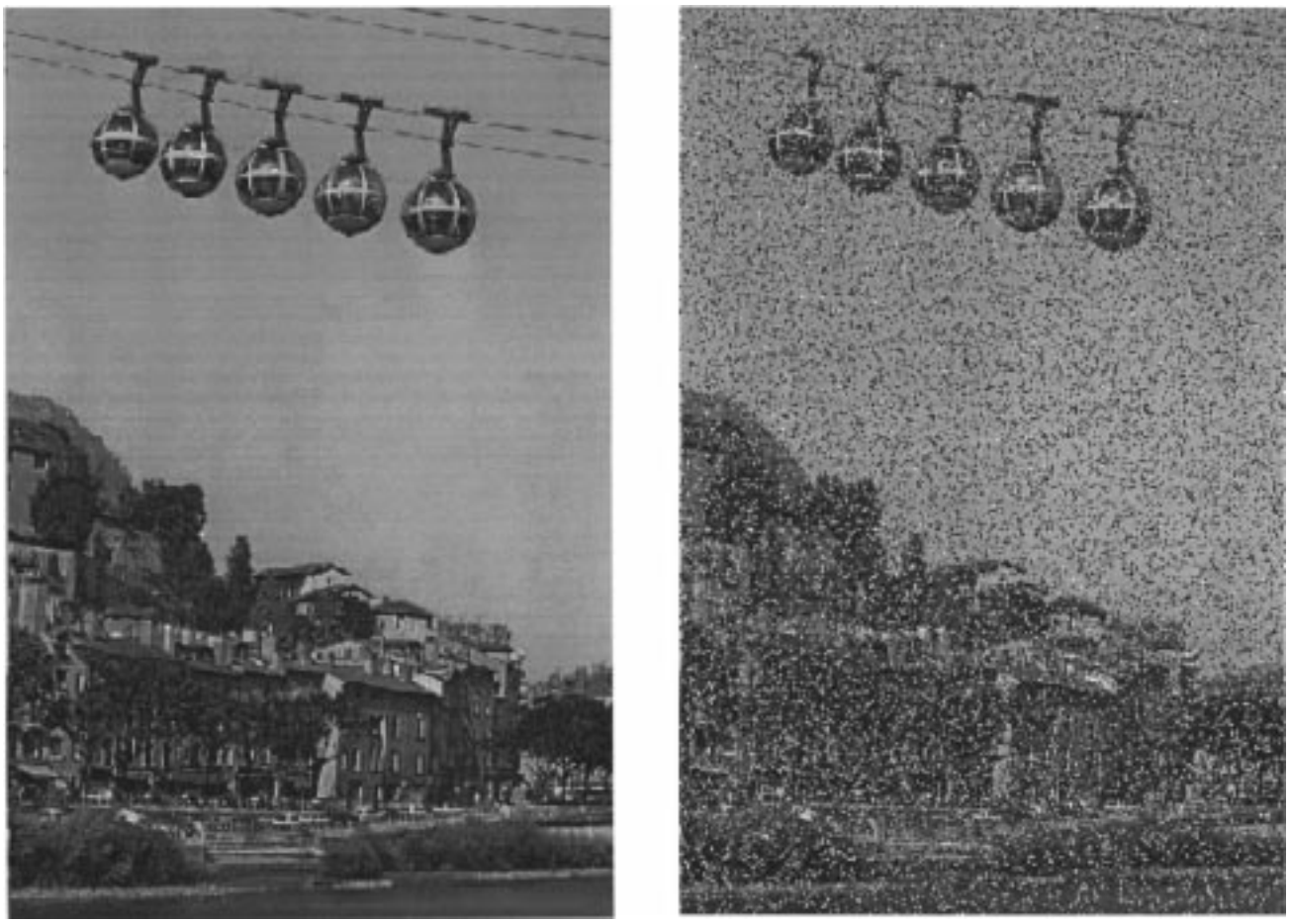

Fig. 5. 512 × 768 landscape image. Left: original image. Right: image with 30% noise.

the segmentation of similar ultrasound images, something which did not seem possible when conventional filters were used [6], [10].

IV. A Related Neural Network

In this section, we will start from a diffusion model which is a variant of (1), (2), (21), and derive a neural network approximation which exhibits learning rules and enjoys nice stability properties. This variant is obtained by removing the thresholding of F in (21), and using instead a saturating coefficient in the diffusion equation (1). More precisely our starting point will be the system

$$\frac{\partial u}{\partial t} - \lambda(u)\mathrm{div}(L\nabla u) = 0 \tag{24}$$

$$\frac{\partial L}{\partial t} + L = \frac{3}{2}(1 - |\nabla u|^2)\mathrm{Id} + |\nabla u|^2 \mathbb{P}_{\nabla u^\perp} \tag{25}$$

where λ is a smooth, positive, even, function satisfying

$$\lambda(u) \to 0 \text{ as } u \to \pm 1$$

and decreasing for $u > 0$ (notice that, for a sake of simplicity, we have chosen $\tau = s = 1$).

Observe that, in this model, the diffusion tensor can actually induce anti-diffusion, where fronts stiffness is larger than $s = 1$, in principle allowing for strong contrast enhancement. The effect of the coefficient λ is to prevent the image from reaching unacceptable high grey levels. Although the mathematical well posedness of this system is far from clear, we think it is of interest in view of the neural network discretization we now describe.

For a sake of simplicity, we will use single index notations: we will denote by x_p the locations of the pixels, or neurons, on a regular lattice of mesh size h and write u_p for the value of u at x_p. We set

$$G(u) = \int_0^u \frac{1}{\lambda(v)}\, dv$$

G is an odd, increasing function. We will assume that

$$G(u) \to \pm\infty \text{ as } u \to \pm 1$$

something which is clearly satisfied, provided the decay of λ to 0 when u tends to ± 1 is fast enough. We then denote by g the reciprocal function of G: it is an increasing, odd function, mapping $\mathbb{R}$ onto $]-1, +1[$. Finally we denote by U the function $G \circ u$.

In the terminology of neural networks u is the output of the network, U its state, and g is the transfer function linking these variables. Typically g is a sigmoid function often chosen as the hyperbolic tangent. Most often a gain parameter, that we will omit here for a sake of simplicity, is used to control the stiffness of this transfer function.

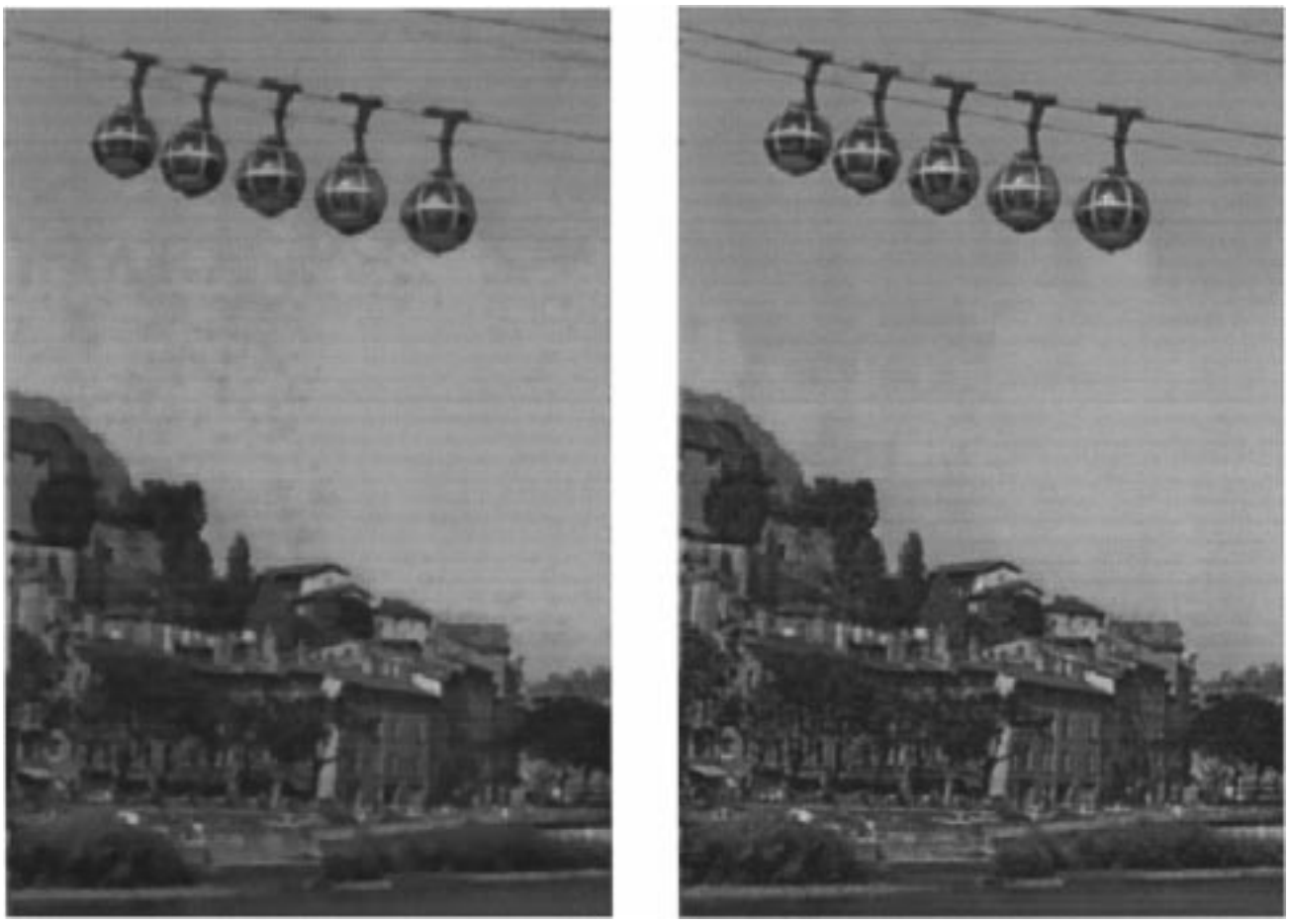

Fig. 5. (*Continued.*) Processed noisy image after zero (left) or one (right) reinitialization. Parameters are $\tau = 10\Delta t$, $s = 5$.

In view of (24), the differential equation satisfied by the state variable U is

$$\frac{dU}{dt} - \text{div}(L\nabla u) = 0. \tag{26}$$

To derive a neural network approximation of (26), the rule is essentially to work on integral approximations of the diffusion operators, then to discretize the integrals on the neurons considered as quadrature points (see [4], [5], [9]).

For a diffusion operator of the form

$$Du = \text{div}(F\nabla u)$$

a general framework is given in [8], where integral approximation are built in the following form:

$$D_\varepsilon v = \int \sigma_\varepsilon(x, y)[v(y) - v(x)]\, dy \tag{27}$$

where

$$\sigma_\varepsilon(x, y) = \varepsilon^{-4} \sum_{i,j} m_{ij}\left(\frac{x+y}{2}\right)\psi_{ij}\left(\frac{y-x}{\varepsilon}\right). \tag{28}$$

In the above formulas, ε is a small parameter, which will be interpreted later as a synaptic range, ψ_{ij} are cut-off functions which need to be related to the functions m_{ij} and the original diffusion tensor L through second-order momentum properties (indices i, j run from one to the dimension of the image, which for the present discussion will be 2).

Several recipes are provided in [8] to actually construct these parameters. Our choice here is a variant of one of these. Let us consider a smooth radially symmetric function θ with compact support (or decaying fast enough at infinity) normalized such that

$$\int_o^\infty r^5\theta(r)\, dr = \frac{4}{\pi}.$$

We take

$$\psi_{ij}(x) = x_i^\perp x_j^\perp \theta(x)$$

where $x_i^\perp$ denotes the ith component of $x^\perp$. One can then show along the same lines as in [8], that is, essentially through order 2 Taylor expansions, that a matrix m leading to a consistent approximation of Du by $D_\varepsilon u$ is given through (28) by

$$m = -F + \tfrac{3}{4}(\text{tr}F)\text{Id} \tag{29}$$

tr$F$ denoting the trace of the matrix F. Applying this construction to our diffusion equation yields functions $\gamma_\varepsilon(x, y, t)$ which have to satisfy

$$\frac{d\gamma_\varepsilon}{dt} + \gamma_\varepsilon = \sigma_\varepsilon$$

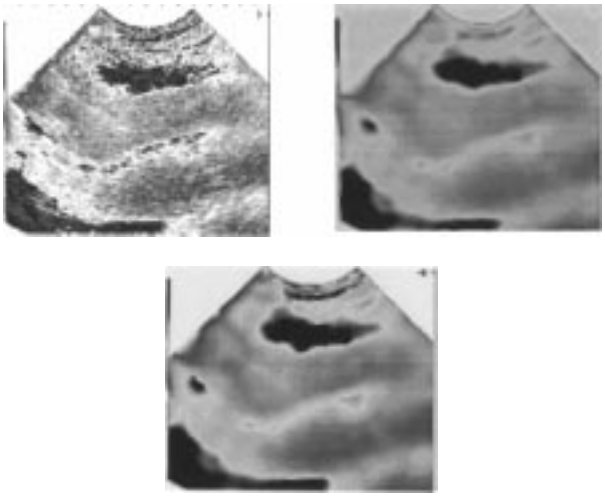

Fig. 6. Ultrasound image. Top-left: original image. Top-right: processed image. Bottom: processed image after one reinitialization.

where σ_ε is derived from the right-hand side F of (25) through (28) and (29). We first observe that

$$\mathrm{tr}F = |\nabla u|^2 + 3(1 - |\nabla u|^2) = 3 - 2|\nabla u|^2.$$

Moreover, if we set $\mathbb{P}_{\nabla u^\perp} = [P_{ij}]$, we have

$$\sum_{i,j} P_{ij}\left(\frac{x+y}{2}\right)(x-y)_i^\perp (x-y)_j^\perp = \frac{1}{\left|\nabla u\left(\frac{x+y}{2}\right)\right|^2}\left|\nabla u\left(\frac{x+y}{2}\right)\cdot(x-y)\right|^2$$

which yields

$$\frac{d\gamma_\varepsilon}{dt}(x,y,t) + \gamma_\varepsilon(x,y,t) = \varepsilon^{-4}\left[\left|\nabla u\left(\frac{x+y}{2}\right)\cdot(x-y)\right|^2 + \frac{3}{4}|y-x|^2\right]\theta\left(\frac{y-x}{\varepsilon}\right).$$

In the above equality, only points x and y within a distance of the order of ε need to be considered, so it is consistent to make the following additional approximation

$$\nabla u\left(\frac{x+y}{2}\right)\cdot(x-y) \simeq u(x) - u(y)$$

and we are left with

$$\frac{d\gamma_\varepsilon}{dt}(x,y,t) + \gamma_\varepsilon(x,y,t) = \varepsilon^{-4}|y-x|^2\theta\left(\frac{y-x}{\varepsilon}\right)\left[\frac{3}{4} - \frac{|u(y)-u(x)|^2}{|y-x|^2}\right].$$

It now remains to do a numerical integration of (27) on quadrature points x_p to obtain the following dynamical system

$$\frac{dU_p}{dt} = h^2 \sum_q \gamma_\varepsilon(x_p, x_q, t)(u_q - u_p) \tag{30}$$

$$\frac{d\gamma_\varepsilon}{dt} + \gamma_\varepsilon = \varepsilon^{-4}|x_q - x_p|^2\theta\left(\frac{x_q - x_p}{\varepsilon}\right)\left[\frac{3}{4} - \frac{|u_q - u_p|^2}{|x_q - x_p|^2}\right]. \tag{31}$$

It is important to point out that this approximation is valid only in the limit of a large number of neurons within the synaptic range.

The system (30), (31) can be interpreted as a neural network dynamic, with learning ability: the synaptic connections, as measured by the coefficients $\gamma_\varepsilon(x_p, x_q, t)$, are enhanced or inhibited, depending on the coherence, evaluated over a time window τ, between neurons p and q as compared to some threshold (which can vary depending on the coefficient s, which we recall was taken equal to 1 in this derivation).

Besides this interpretation, which sheds a different light on our PDE model, one nice feature of the system (30), (31) is that it is possible to construct for it a Lyapunov function [17]. Let us denote by Σ the time-dependent vector $(\gamma_{pq}) = \gamma_\varepsilon(x_p, x_q)$ and set

$$a_{pq} = \varepsilon^{-4}|x_q - x_p|^2\theta\left(\frac{x_q - x_p}{\varepsilon}\right); \quad b_{pq} = |x_q - x_p|^{-2}$$

and

$$H(u,\Sigma) = \tfrac{1}{2}\sum_{p,q}\gamma_{pq}^2 + \sum_{p,q}\gamma_{pq}\left[b_{pq}(u_p - u_q)^2 - \tfrac{3}{4}\right].$$

We have

$$\frac{dH}{dt} = \sum_{p,q}\gamma_{pq}\frac{d\gamma_{pq}}{dt} + \sum_{p,q}\frac{d\gamma_{pq}}{dt}\left[b_{pq}(u_p - u_q)^2 - \frac{3}{4}\right] + 2\sum_{p,q}\gamma_{pq}b_{pq}(u_p - u_q)\left(\frac{du_p}{dt} - \frac{du_q}{dt}\right).$$

Using (31), we obtain

$$\frac{dH}{dt} = -\sum_{p,q}\left(\frac{d\gamma_{pq}}{dt}\right)^2 + 2\sum_{p,q}\gamma_{pq}b_{pq}\left(u_p\frac{du_p}{dt} + u_q\frac{du_q}{dt} - u_q\frac{du_p}{dt} - u_p\frac{du_q}{dt}\right).$$

We then observe that, due to (31) and the symmetry of θ, $\gamma_{pq} = \gamma_{qp}$, which allows to rewrite the second sum in the right hand side above as

$$2\sum_{p,q}\gamma_{pq}\frac{du_p}{dt}(u_p - u_q)b_{pq}$$

and thus, from (30),

$$\frac{dH}{dt} = -\sum_{p,q}\left(\frac{d\gamma_{pq}}{dt}\right)^2 - 4\sum_{p,q}\gamma_{pq}b_{pq}\left(\frac{du_p}{dt}\right)^2\frac{1}{g'(u_p)}. \tag{32}$$

Therefore

$$\frac{dH}{dt} \le 0.$$

We next observe that, by definition, u remains between -1 and $+1$ and thus γ_{pq} is bounded. As a result, when $t \to \infty$ $H(u,\Sigma)$ tends to a minimum, where $dH/dt = 0$. Moreover it results from (32) that, at such point, one must have

$$\frac{d\gamma_{pq}}{dt} = 0 \text{ and } \frac{du_p}{dt} = 0$$

for all p, q. In other words, the dynamical system (30), (31) tends to a steady state.

We performed some numerical experiments that confirm this theoretical result together with the contrast enhancement ability of this model. However, this model only produces binary asymptotic images, which in our opinion makes it less flexible for general applications than the original PDE system (1) and (2).

V. Conclusion

We have presented a nonlinear diffusion model for image restoration that combines time-delay regularization and anisotropic diffusion. Partial results concerning its well-posedness have been proved. The links of the model with natural neural networks with desirable stability properties have been demonstrated. The model allows to select the steady states that will be obtained on the processed images on the basis of a contrast parameter. An iterative strategy allows to remove the dependence of the model on the choice of the initial diffusion tensor. Numerical examples illustrate its ability to remove large amounts of noise while keeping small scale details of the image. This feature makes the model suitable for preprocessing highly degraded images in order to allow segmentation techniques to be successfully used.

References

[1] L. Alvarez, F. Guichard, P.-L. Lions, and J.-M. Morel, "Axioms and fundamental equations in image processing," *Arch. Rational Mech. Anal.*, vol. 123, pp. 199–257, 1993.

[2] L. Alvarez, P.-L. Lions, and J.-M. Morel, "Image selective smoothing and edge detection by nonlinear diffusion II," *SIAM J. Numer. Anal.*, vol. 29, pp. 845–866, 1992.

[3] F. Catté, J.-M. Morel, P.-L. Lions, and T. Coll, "Image selective smoothing and edge detection by nonlinear diffusion," *SIAM J. Numer. Anal.*, vol. 29, pp. 182–193, 1992.

[4] G.-H. Cottet, "Modèles de réaction-diffusion pour des réseaux de neurones stochastiques et déterministes," *C. R. Acad. Sci. Paris*, vol. 312, 1991.

[5] ———, "Neural networks: Continuous approach and applications to image processing," *J. Biol. Syst.*, vol. 3, pp. 1131–1139, 1995.

[6] G.-H. Cottet and M. El Ayyadi, "Nonlinear PDE operators with memory terms for image processing," in *Proc. Third IEEE Int. Conf. Image Processing*, 1996, pp. I-481–I-484.

[7] G.-H. Cottet and L. Germain, "Combining nonlinear diffusion with reaction for image processing," *Math. Comput.*, vol. 61, pp. 659–673, 1993.

[8] P. Degond and S. Mas-Gallic, "The weighted particle method for convection-diffusion equations. II: The anisotropic case," *Math. Comput.*, vol. 53, pp. 485–508, 1989.

[9] R. Edwards, "Approximation of neural network dynamics by reaction-diffusion equations," *Math. Methods Appl. Sci.*, vol. 19, pp. 651–677, 1996.

[10] M. El Ayyadi, F. Leitner, G.-H. Cottet, and J. Demongeot, "Image segmentation using snake-splines and nonlinear diffusion operators," preprint, 1995.

[11] M. Nitzberg, D. Mumford, and T. Shiota, "Filtering, segmentation and depth," in *Lecture Notes in Computer Science*, vol. 662. New York: Springer-Verlag, 1993.

[12] P. Perona and J. Malik, "Scale space and edge detection using anisotropic diffusion," *IEEE Trans. Pattern Anal. Machine Intell.*, vol. 12, pp. 629–630, 1990.

[13] L. I. Rudin, S. Osher, and E. Fatemi, "Nonlinear total variation based noise removal algorithms," *Physica-D*, vol. 60, pp. 259–268, 1992.

[14] J. Shah, "A common framework for curve evolution, segmentation and anisotropic diffusion," in *IEEE Conf. Computer Vision and Pattern Recognition*, 1996.

[15] J. Weickert, "Scale-space properties of nonlinear diffusion filtering with a diffusion tensor," preprint, 1994.

[16] ———, "Anisotropic diffusion in image processing," Ph.D. dissertation, Univ. Kaiserslautern, Germany, 1996.

[17] D. Zaharie, personal communication.

Georges Henri Cottet received the Ph.D. degree in applied mathematics from Ecole Polytechnique, Paris, France, in 1982. He received the Thèse d'Etat in 1987.

From 1982 to 1990, he worked at the Centre Nationale de Recherche Scientifique, and joined the University of Grenoble, France, as a Professor in 1990. His research interests are in numerical analysis, in particular the fields of computational fluid dynamics, neural networks, and image processing.

Mohamed El Ayyadi received the M.S. and Ph.D. degrees in applied mathematics from the University of Grenoble, France, in 1993 and 1997, respectively.

He is currently a post-doctoral fellow at Washington University Medical Center, St. Louis, MO. His research interests include applications of PDE's and neural networks in image processing.